Tuning of magnetic and transport properties in Bi₂Te₃ by divalent Fe doping

N. H. Jo,[1] K. J. Lee,[1] C. M. Kim,[1] K. Okamoto,[2] A. Kimura,[2] K. Miyamoto,[3] T. Okuda,[3] Y. K. Kim,[4] Z. Lee,[4]
T. Onimaru,[5] T. Takabatake,[5] and M. H. Jung[1,*]

[1]*Department of Physics, Sogang University, Seoul 121-742, Republic of Korea*
[2]*Graduate School of Science, Hiroshima University, 1-3-1 Kagamiyama, Higashi-Hiroshima 739-8526, Japan*
[3]*Hiroshima Synchrotron Radiation Center, Hiroshima University, 2-313 Kagamiyama, Higashi-Hiroshima 739-0046, Japan*
[4]*School of Mechanical & Advanced Materials Engineering, UNIST, Ulsan 689-798, Republic of Korea*
[5]*Department of Quantum Matter, ADSM, Hiroshima University, 1-3-1 Kagamiyama, Higashi-Hiroshima 739-8530, Japan*

We report the doping effect of a magnetic Fe ion in Bi₂Te₃, that is, $Bi_{2-x}Fe_xTe_3$ ($x = 0$, 0.08, 0.15, 0.2, 0.25, and 0.3). The paramagnetic magnetization data reveal that the Fe ions are doped in the divalent form. The Fe^{2+} state substituted for Bi^{3+} can create hole donors, which compensate for the electron dopants of Bi₂Te₃ with a small amount of Te excess. This causes the n-type carrier density to be decreased with increasing x, and finally be changed to p type at $x = 0.3$, where the carrier mobility suddenly drops and the electrical resistivity abruptly increases. These results are consistent with angle-resolved photoemission spectroscopy experiments. The Fermi level shifts downward with increasing x. Furthermore, we find a larger spin polarization for the Fe-doped Bi₂Te₃ samples, which is crucial for future spintronics applications.

Bi₂Te₃ is not only a traditional material of the A_2B_3 ($A =$ Bi, Sb and $B =$ Se, Te) family to show high thermoelectric efficiency at room temperature,[1–3] but also a new material of three-dimensional topological insulators to show an insulating bulk band with a metallic surface state.[4] The surface state, protected by time-reversal symmetry, has been theoretically predicted from band calculations[5–8] and experimentally ascertained from angle-resolved photoemission spectroscopy (ARPES).[9–12] The two-dimensional transport arising from the topological surface state is expected to be useful for potential device applications.[13,14] However, it is difficult to observe the surface state by measuring the electrical transport because of the large number of antisite defects between the Bi and Te sites in Bi₂Te₃.[15–20] If Bi₂Te₃ samples are prepared from stoichiometric melts, p-type charge carriers are invariably generated due to the presence of Bi$_{Te}$-type antisite defects, i.e., some atoms of Bi occupying the Te sublattice.[18] On the other hand, when an excess of Te is introduced into Bi₂Te₃, the antisite defects of type Te$_{Bi}$ become dominant.[19,20] Then, n-type charge carriers are generated so that the Fermi level often touches the bulk conduction band. In this case, the carrier density reaches up to $\sim 10^{19}$ cm^{-3} in the bulk regime. If monovalent or divalent ions are replaced for the trivalent Bi ions, the charge carriers can be tuned to be p type after passing through the topological surface regime. Moreover, if the doped ion is magnetic, the time-reversal symmetry can be broken to open a gap because of the magnetic order.[21–23]

In this Rapid Communication, we report the doping effect of magnetic Fe in Bi₂Te₃, that is, $Bi_{2-x}Fe_xTe_3$ ($x = 0$, 0.08, 0.15, 0.20, 0.25, and 0.3). The single crystals are prepared with a small amount of Te excess, which causes antisite defects of type Te$_{Bi}$, leading to the generation of n-type charge carriers. The Fe doping drives the tuning of charge carriers from n to p type at $x = 0.3$, where the carrier mobility is suddenly suppressed. From the fit with the Brillouin function of the magnetization versus field curve in Fe-doped Bi₂Te₃, the valence of the Fe state is divalent. This indicates that

Fe doping can create hole donors, which compensate for the electron dopants from antisite defects of type Te$_{Bi}$, so that the n-type carrier density is decreased with an increase of the Fe contents up to $x = 0.25$. This result is well consistent with the result of ARPES experiments. For an Fe content of $x = 0.3$, the hole carriers become dominant and the carrier density is more suppressed. The Fe doping effect is more explicit in magnetic properties, which undergo paramagnetic behavior, as compared with other reports on ferromagnetic order at low temperatures.[23]

The single crystals of $Bi_{2-x}Fe_xTe_3$ ($x = 0$, 0.08, 0.15, 0.20, 0.25, and 0.3) were prepared by a congruent melting method. A stoichiometric mixture of Bi, Fe, and Te with a small amount of Te excess was put into a cleaned quartz tube and sealed in vacuum. The temperature was slowly raised up to 800 °C and kept for 16 h. Then it was slowly cooled down to 550 °C and kept for 3 days. This annealing process was required to obtain pure crystals. All the grown crystals were well cleaved along the basal plane. The cleaved surface was silvery, shiny, and mirrorlike. The transport and magnetic properties were measured by using the physical property measurement system (PPMS) and a superconducting quantum interference device–vibrating sample magnetometer (SQUID-VSM), respectively. The spin-resolved ARPES measurement was performed with a He discharge lamp at the efficient spin-resolved spectroscopy end station of the Hiroshima synchrotron radiation center.[24] The measurement was performed at 8 K, and the sample was *in situ* cleaved under an ultrahigh vacuum below 1×10^{-8} Pa.

The crystals were characterized by imaging, spectroscopic, and diffractive methods. Aberration-corrected scanning transmission electron microscope (STEM) images of cross-sectional Bi₂Te₃ in Fig. 1(a) clarify that the atomic lattice fringes are clearly visible and the lattice spacing is 0.579(4) nm, in good agreement with the d value of (101) planes of the rhombohedral Bi₂Te₃ samples.[25] In Fig. 1(b), the atomic resolution STEM images present identical atomic
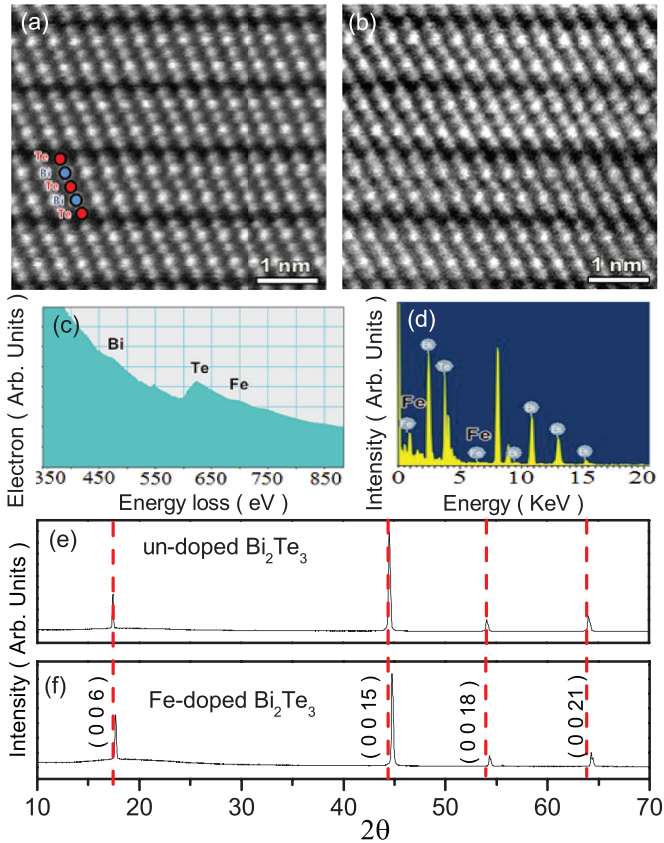
FIG. 1. (Color online) (a), (b) Aberration-corrected scanning transmission electron microscope (STEM) images of the $x = 0$ and 0.08 samples. For the $x = 0.08$ sample: (c) electron energy loss spectroscopy (EELS) and (d) energy dispersive spectroscopy (EDS). (e), (f) X-ray diffraction (XRD) data of the $x = 0.08$ samples.

structures even with Fe doping in the $x = 0.08$ sample. In the spectroscopic studies of the $x = 0.08$ sample of Figs. 1(c) and 1(d), the Fe L_3 and L_2 edges in electron energy loss spectroscopy (EELS) and Fe $K\alpha$ edge in energy dispersive spectroscopy (EDS) indicate the presence of Fe in the lattices of the $x = 0.08$ sample. These results support that Fe is indeed substituted in Bi_2Te_3. Figures 1(e) and 1(f) show the x-ray diffraction (XRD) patterns measured on the cleaved surface for two typical samples of $x = 0$ and 0.08. The diffraction peaks are exclusively labeled with (00L) indices without any impurity peaks. This indicates that the samples are single crystalline and the cleaved surface is perpendicular to the c axis. The obtained c-axis lattice parameter for the $x = 0$ sample is 30.47 Å, which is the same value reported by other literature[26] and is larger than the value obtained for the $x = 0.08$ sample. It is expected when considering the smaller ionic radius of Fe than of Bi. These characterized data for the other samples are not shown here because they have a similar tendency.

With these well characterized single crystals, first we determine the carrier type and the carrier density from the slope of the Hall resistance, and then the carrier mobility is calculated with the obtained carrier density and electrical resistivity. The electrical resistivity data will be discussed later. In Table I, we summarize the carrier type and the values of
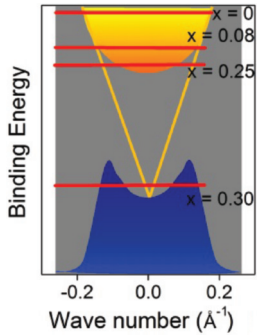
the carrier density, electrical resistivity, and carrier mobility obtained at 3 K. The $x = 0$ sample is simply n type with a carrier density of 8.03×10^{18} cm^{-3}, which decreases with increasing Fe contents to be 3.36×10^{18} cm^{-3} for $x = 0.25$. For the highest doping content of $x = 0.3$, the carrier type is changed to p type with a carrier density of 2.02×10^{18} cm^{-3}. These carrier density values are still in the bulk regime. When the carrier type is n type ($x < 0.3$), the carrier mobility is almost the same, while the carrier mobility is suddenly suppressed for the p-type sample ($x = 0.3$). Here it should be mentioned that in the $x = 0.3$ sample the electrical resistivity is also suddenly changed from metallic behavior, which will be discussed later in Fig. 4. With these values listed in Table I, we plot the hypothetical band structure with different positions of the Fermi level for each sample. As expected, the Fermi level of the $x = 0$ sample with an excess of Te is located in the bulk conduction band because of Te$_{Bi}$-type antisite defects. The Fermi level of Fe-doped Bi_2Te_3 samples is continuously lowered with increasing Fe contents x. When the Fermi level is in the bulk conduction band regime ($x = 0$–0.25), the n-type carrier density is decreased by Fe doping. On the other hand, when the Femi level is in the bulk valence band regime ($x = 0.3$), the surface carriers may be screened by the p-type carriers from the bulk valence band, leading to a strong suppression of carrier mobility.

To confirm the location of the Fermi level, we carried out ARPES experiments. Figures 2(a) and 2(b) show the results of energy dispersion curves along the K-Γ-K line of the $x = 0$ and 0.08 samples, respectively. Unfortunately, we do not have the ARPES data for higher x value samples. In Fig. 2, the topological surface state with a linear dispersion is clearly visible. The overall features shown here for the $x = 0$ sample are quite similar to those previously reported for Bi_2Te_3.[12] A conduction band is enclosed inside the topological surface state and crosses the Fermi energy, supporting the n-type carrier conduction in these samples. The noticeable feature is that the Fe doping lowers the Fermi level, as predicted by the transport results. In the upper panels of Figs. 2(a) and 2(b), the constant energy contours at the binding energy of $E_B = 100$ meV are similar so as to be hexagonally warped, which agrees well with other reports.[12] Here a question arises: How much is the spin polarization affected by the Fe doping? Although the theoretically derived spin polarization is above 50% for Bi_2Te_3,[27] the reported values are much lower by about 20%.[4,28] Figures 2(c) and 2(d) show the spin-resolved energy distribution curves measured at emission angles of $\pm 3°$ which correspond to $k = -0.1$ and $+0.1$ Å^{-1}, respectively, as denoted by the two dots in the upper panel of Fig. 2(b). Prominent spin-up and spin-down features are clearly seen around $E_B = 100$ meV, where their signs are opposite for $k = -0.1$ and $+0.1$ Å^{-1}. The observed spin polarizations are 60% for the $x = 0$ sample and 75% for the $x = 0.08$ sample. This larger spin polarization is crucial for future spintronics applications.

In order to probe the spin states affected by Fe doping, we have measured the magnetization versus magnetic field curves. In a previous report,[24] Bi_2Te_3 becomes ferromagnetic by Fe doping. The Curie temperature is between 9 and 12 K, and the easy magnetization direction is the c axis. However, in our case we find that Bi_2Te_3 is diamagnetic and all the Fe-doped

TABLE I. (Color online) Values of carrier density, electrical resistivity, and carrier mobility measured at 3 K for Bi_2Te_3 ($x = 0$) and Fe-doped Bi_2Te_3 ($x = 0.08$, 0.15, 0.20, 0.25, and 0.3). The figure in the right-hand column shows the hypothetical band structure with different positions of the Fermi level (red lines) for each sample.

Material (Bi_2Te_3)	Carrier type	Carrier density (10^{18} cm^{-3})	Resistivity ($\mu\Omega$ cm)	Mobility (cm^2 V^{-1} s^{-1})
Bi_2Te_3 ($x = 0$)	n	8.03	27.5	28293.09
Fe doped ($x = 0.08$)	n	5.29	35.2	33480.33
Fe doped ($x = 0.15$)	n	3.80	51.4	32010.65
Fe doped ($x = 0.20$)	n	3.95	81.0	19522.01
Fe doped ($x = 0.25$)	n	3.36	116.7	15941.37
Fe doped ($x = 0.30$)	p	2.02	26300	117.54

Bi_2Te_3 is paramagnetic. In Fig. 3, the total magnetization is increased with increasing Fe contents, implying that the Fe atoms are nominally well doped into Bi_2Te_3. However, if the magnetization is subtracted by the diamagnetic background signal, the magnetization for (n-type) $x < 0.3$ samples is still increased with increasing x except for the (p-type) $x = 0.3$ sample, where the carrier type is changed, the carrier mobility suddenly drops, and the electrical resistivity abruptly increases. The magnetization curve for the $x = 0.3$ sample shows no magnetic hysteresis, indicating that the $x = 0.3$ sample is indeed paramagnetic. The sudden increase of the

low-field magnetization data are well fitted by the Brillouin function with a divalent Fe state, which is shown as the solid line in Fig. 3. This result is consistent with that expected from the transport properties. The Fe^{2+} state substituted for Bi^{3+} can create hole donors, which compensate for the inherent electrons. Thus, with increasing x values up to 0.25, the n-type carrier density is decreased, and finally the carrier density is changed to p type at $x = 0.3$.

Now let us discuss the electrical resistivity data plotted in Fig. 4. For the n-type samples ($x = 0$, 0.08, 0.15, 0.20, and 0.25), the electrical resistivity monotonically decreases with
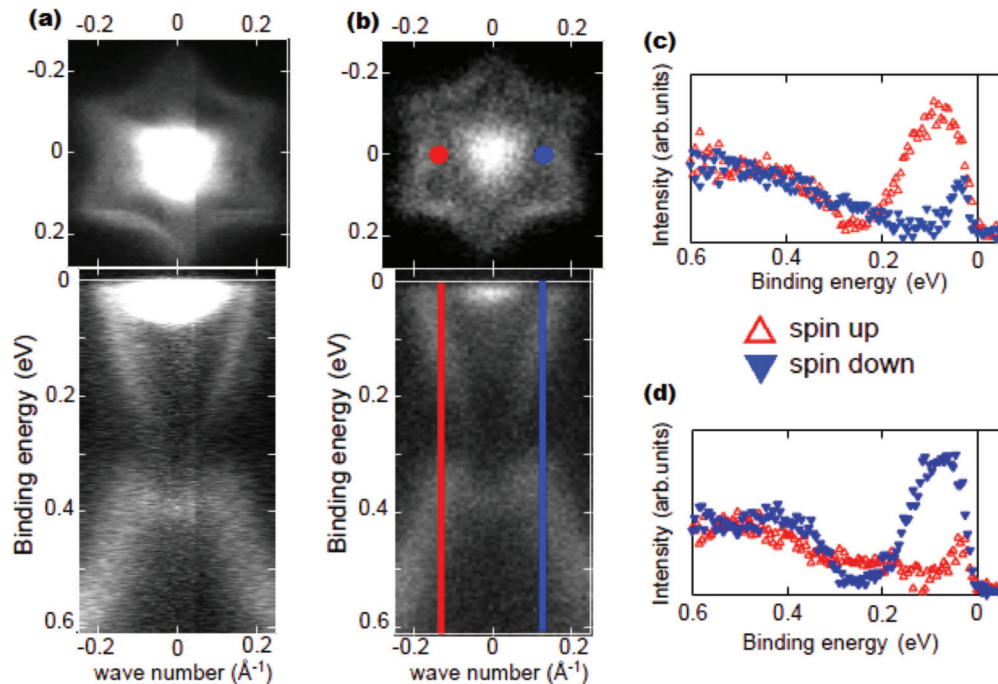

FIG. 2. (Color online) (a), (b) Constant energy contour and energy dispersion curves of the $x = 0$ and 0.08 samples. The position of the Fermi energy shifts downward by Fe doping. (c), (d) Spin-resolved energy distribution curves taken at $k = -0.1$ Å^{-1} corresponding to the red symbol and red line in (b) and $k = +0.1$ Å^{-1} corresponding to the blue symbol and blue line in (b). The spin-up and spin-down features are clearly antisymmetric for $k = -0.1$ and $+0.1$ Å^{-1}.

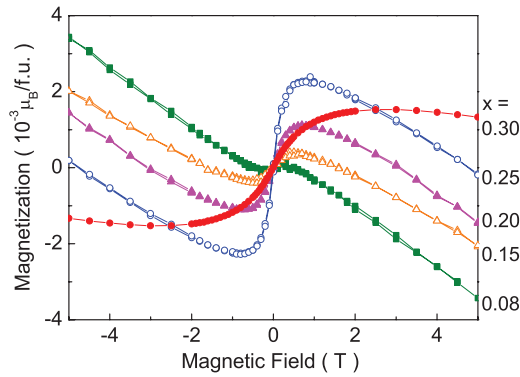FIG. 3. (Color online) Magnetization vs field for the $x = 0.08$, 0.15, 0.2, 0.25, and 0.3 samples.
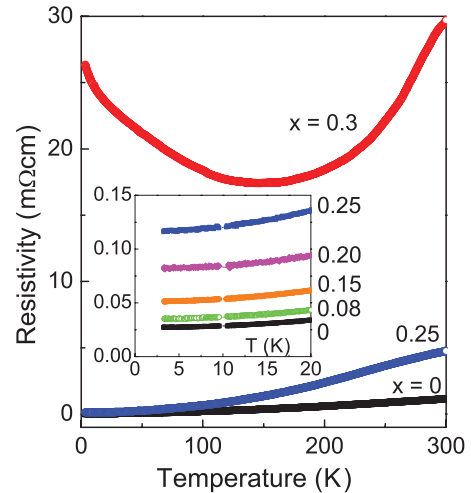

FIG. 4. (Color online) Electrical resistivity vs temperature for the $x = 0$, 0.25, and 0.3 samples. The inset shows the low-temperature data for the $x = 0$, 0.08, 0.15, 0.2, and 0.25 samples.

decreasing temperature. The inset shows the low-temperature data for a comparison. This is typical metallic behavior, because the Fermi level is located in the bulk conduction regime. However, at the p-type sample ($x = 0.3$), the electrical resistivity is an order of three times larger than that of the other samples and undergoes a semiconducting behavior at low temperatures below 150 K. This semiconducting behavior may come from the reduction of antisite defects in our system, or the topological transport properties as reported by Qu *et al.*.[29] However, it should be mentioned that the carrier density of the $x = 0.3$ sample is in the bulk regime. We expect that such a high resistivity value may come from the mixture of the bulk valence band and topological surface state, because the Fermi level spans the bulk valence band with the topological surface state, as shown in the band structure of Table I. Then, we can expect a p-type bulk carrier density of the order of 10^{18} cm^{-3} with a low density of surface electrons, which hinder the movement of charge carriers. Because we detected the mobility of bulk carriers from our simple Hall measurements, the carrier mobility precipitously drops in the $x = 0.3$ sample.

In conclusion, by introducing divalent Fe ions instead of trivalent Bi ions in Bi_2Te_3, we have achieved a change in carrier type from electrons to holes at $x = 0.3$ in $Bi_{2-x}Fe_xTe_3$,

where the carrier mobility suddenly drops and the electrical resistivity abruptly increases. The n-type carrier density is decreased with increasing Fe contents; from 8.03×10^{18} cm^{-3} for $x = 0$ to 3.36×10^{18} cm^{-3} for $x = 0.25$. This result is reconfirmed by angle-resolved photoemission spectroscopy experiments. The decrease of n-type carriers is attributed to the hole donors created from divalent Fe ions substituted for trivalent Bi ions. The Fe^{2+} states are demonstrated by the fit of magnetization versus field curves with a Brillouin function form. We observe paramagnetic behavior for Fe-doped Bi_2Te_3, as compared with previous reports. In addition, we find a larger spin polarization for Fe-doped Bi_2Te_3, which is beneficial for spintronics applications.

*Corresponding author: mhjung@sogang.ac.kr

[1] H. J. Goldsmid and R. W. Douglas, Br. J. Appl. Phys. **5**, 386 (1954).

[2] R. Venkatasubramanian, E. Siivola, T. Colpitts, and B. O'Quinn, Nature (London) **413**, 597 (2001).

[3] C. M. Bhandari, H. Scherrer, S. Scherrer, and G. A. Slack, in *CRC Handbook of Thermoelectrics*, edited by D. M. Rowe (CRC, Boca Raton, FL, 1995), Chaps. 6, 19, and 34.

[4] M. Z. Hasan and C. L. Kane, Rev. Mod. Phys. **82**, 3045 (2010).

[5] H. Zhang, C.-X. Liu, X.-L. Qi, X. Dai, Z. Fang, and S.-C. Zhang, Nat. Phys. **5**, 438 (2009).

[6] C. L. Kane and E. J. Mele, Phys. Rev. Lett. **95**, 126802 (2005).

[7] C. L. Kane and E. J. Mele, Science **314**, 1692 (2006).

[8] L. Fu, L. Kane, and E. J. Mele, Phys. Rev. Lett. **98**, 106803 (2007).

[9] D. Hsieh, D. Qian, L. Wray, Y. Xia, Y. S. Hor, R. J. Cava, and M. Z. Hasan, Nature (London) **452**, 970 (2008).

[10] D. Hsieh, Y. Xia, L. Wray, D. Qian, A. Pal, J. H. Dil, J. Osterwalder, F. Meier, C. L. Kane, Y. S. Hor, R. J. Cava, and M. Z. Hasan, Science **323**, 919 (2009).

[11] Y. Xia, D. Qian, D. Hsieh, L. Wray, A. Pal, H. Lin, A. Bansil, D. Grauer, Y. S. Hor, R. J. Cava, and M. Z. Hasan, Nat. Phys. **5**, 398 (2009).

[12] Y. L. Chen, J. G. Analytis, J.-H. Chu, A. K. Liu, S.-K. Mo, X. L. Qi, H. J. Zhang, D. H. Lu, X. Dai, Z. Fang, S. C. Zhang, I. R. Fisher, Z. Hussain, and Z.-X. Shen, Science **325**, 178 (2009).

[13] D. Pesin and A. H. MacDonald, Nat. Mater. **11**, 409 (2012).

[14] I. Vobornki, U. Manju, J. Fujii, F. Borgatti, P. Torelli, D. Krizmancic, Y. S. Hor, R. J. Cava, and G. Panaccione, Nano Lett. **11**, 4079 (2011).

[15]T. C. Harman, B. Paris, S. E. Miller, and H. L. Goering, J. Phys. Chem. Solids **2**, 181 (1957).

[16]A. Hashibon and C. Elsasser, Phys. Rev. B **84**, 144117 (2011).

[17]C. B. Satterthwaite and R. W. Ure. Jr., Phys. Rev. **108**, 1164 (1957).

[18]G. R. Miller and C. Y. Li, J. Phys. Chem. Solids **26**, 173 (1965).

[19]R. F. Brebrick, J. Phys. Chem. Solids **30**, 719 (1969).

[20]S. Cho, Y. Kim, A. Divenere, G. K. Wong, J. B. Ketterson, and J. R. Meyer, Appl. Phys. Lett. **75**, 1401 (1999).

[21]L. A. Wray, S.-Y. Xu, Y. Xia, D. Hsieh, A. V. Fedorov, Y. S. Hor, R. J. Cava, A. Bansil, H. Lin, and M. Z. Hasan, Nat. Phys. **7**, 32 (2011).

[22]Y. Okada, C. Dhital, W. Zhou, E. D. Huemiller, H. Lin, S. Basak, A. Bansil, Y. B. Huang, H. Ding, Z. Wang, S. D. Wilson, and V. Madhavan, Phys. Rev. Lett. **106**, 206805 (2011).

[23]Y. L. Chen, J.-H. Chu, J. G. Analytis, Z. K. Liu, K. Lgarashi, H.-H. Kuo, X. L. Ui, S. K. Mo, R. G. Moore, D. H. Ju, M. Hashimoto, T. Sasagawa, S. C. Zhang, I. R. Fisher, Z. Hussain, and Z. X. Shen, Science **329**, 659 (2010).

[24]V. A. Kul'bachinskii, A. Y. Kaminskii, K. Kindo, Y. Narumi, K. Suga, P. Lostak, and P. Svanda, JETP Lett. **73**, 352 (2001).

[25]T. Okuda, K. Miyamaoto, H. Miyahara, K. Kuroda, A. Kimura, H. Namatame, and M. Taniguchi, Rev. Sci. Instrum. **82**, 103302 (2011).

[26]S. M. Souza, D. M. Triches, C. M. Poffo, J. C. De Lima, T. A. Grandi, and R. S. De Biasi, J. Appl. Phys. **109**, 013512 (2011).

[27]O. V. Yazyev, J. E. Moore, and S. G. Louie, Phys. Rev. Lett. **105**, 266806 (2010).

[28]D. Hsieh, Y. Xia, D. Qian, L. Wray, J. H. Dil, F. Meier, J. Osterwalder, L. Patthey, J. G. Checkelsky, N. P. Ong, A. V. Fedorov, H. Lin, A. Bansil, D. Grauer, Y. S. Hor, R. J. Cava, and M. Z. Hasan, Nature (London) **460**, 1101 (2009).

[29]D.-X. Qu, Y. S. Hor, J. Xiong, R. J. Cava, and N. P. Ong, Science **329**, 821 (2010).